Long Wavelength Coherent Pulse of Sound Propagating in Granular Media

Rohit Kumar Shrivastava, Amalia Thomas, Nathalie Vriend, Stefan Luding

Abstract—A mechanical wave or vibration propagating through granular media exhibits a specific signature in time. A coherent pulse or wavefront arrives first with multiply scattered waves (coda) arriving later. The coherent pulse is micro-structure independent i.e. it depends only on the bulk properties of the disordered granular sample, the sound wave velocity of the granular sample and hence bulk and shear moduli. The coherent wavefront attenuates (decreases in amplitude) and broadens with distance from its source. The pulse attenuation and broadening effects are affected by disorder (polydispersity; contrast in size of the granules) and have often been attributed to dispersion and scattering. To study the effect of disorder and initial amplitude (non-linearity) of the pulse imparted to the system on the coherent wavefront, numerical simulations have been carried out on one-dimensional sets of particles (granular chains). The interaction force between the particles is given by a Hertzian contact model. The sizes of particles have been selected randomly from a Gaussian distribution, where the standard deviation of this distribution is the relevant parameter that quantifies the effect of disorder on the coherent wavefront. Since, the coherent wavefront is system configuration independent, ensemble averaging has been used for improving the signal quality of the coherent pulse and removing the multiply scattered waves. The results concerning the width of the coherent wavefront have been formulated in terms of scaling laws. An experimental set-up of photoelastic particles constituting a granular chain is proposed to validate the numerical results.

Keywords—Discrete elements, Hertzian Contact, polydispersity, weakly nonlinear, wave propagation.

I. Introduction

SOUND propagation through particulate media (granular matter) has been a helpful tool in capturing the material properties through which it is propagating. This attribute has been extensively used for seismic exploration of oil/gas/mineral reservoirs [1], studying the internal structure of a planetary body (Moon / Earth, [2]) or for geotechnical investigations to determine the material properties [3]. There are various phenomena associated with sound propagation like multiple scattering, attenuation, geometric spreading, dispersion, coherent back scattering effects, wave localization, etc. [4]. These individual phenomena allow us to measure, evaluate and predict the material properties and, hence, enable

S. Luding is with Multiscale Mechanics (MSM), MESA+, Engineering Technology (ET), P.O. Box 217, 7500 AE Enschede, The Netherlands.

R. K. Shrivastava is with Multiscale Mechanics (MSM), MESA+, Engineering Technology (ET), P.O. Box 217, 7500 AE Enschede, The Netherlands (e-mail: r.k.shrivastava@utwente.nl).

N. Vriend is with Environmental and Industrial Fluid Dynamics, DAMTP, Centre for Mathematical Sciences, Wilberforce Road, Cambridge, CB3 0WA, United Kingdom.

A. Thomas is with Environmental and Industrial Fluid Dynamics, DAMTP, Centre for Mathematical Sciences, Wilberforce Road, Cambridge, CB3 0WA, United Kingdom (e-mail: at682@damtp.cam.ac.uk).
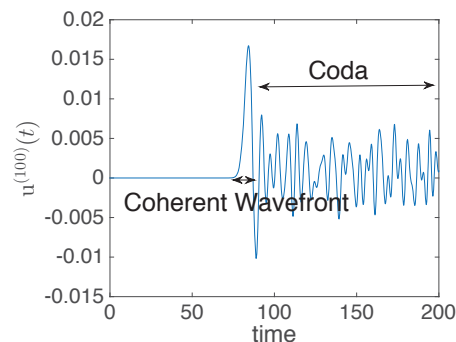
Fig. 1 Wave propagating in a one-dimensional chain; displacement response of 100th particle, initial impulse $v_o = 0.1$ plotted against dimensionless time (Section II), disorder parameter $\xi = 0.2$ (Section II-E)

us to study the material without destroying it (non-destructive testing).

The space time responses of the particles through which the mechanical wave is propagating has a typical signature of its own [5]-[7]. The signal has a coherent wave front as the first arrival (in terms of time) and is accompanied by the multiply scattered waves (coda) as shown in the illustration (Fig. 1). The coherent wave has long wavelength and low frequency property and the coda has the vice-versa. The multiply scattered part of the signal is extremely phobic to averaging and gets completely removed. The coherent wavefront maintains its shape(width) and size (amplitude) on ensemble averaging in comparison to the signal from a single realization [8]. This property indicates that the coherent wavefront contains information regarding the bulk property of the system, e.g. bulk moduli, shear moduli, primary wave velocity (P-wave), co-ordination number, etc. [9].

In Ref. [5], it is shown that the propagating coherent wavefront (pulse) attenuates and "broadens" as it propagates along a medium, this "broadening" is affected by the disorder in particle sizes as well as by the propagation length. We investigate this observation and found some agreements with the scaling parameters observed in [5]. This observation indicates a potential application for determining the structure or the granular size distribution of the medium. However, in [10], it was observed that the space time responses for a set of particles with nonlinear repulsive interaction force (when the amplitude of the propagating wave is high) are significantly different from the ones obtained when the inter-particle forces are linear in nature even if there is no opening and closing of contacts (non-occurrence of sonic vacuum, [11]). The aforementioned observation and the previous work
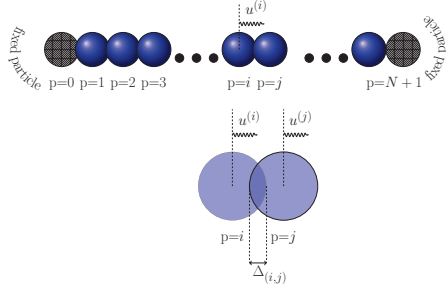
Fig. 2 Schematic diagram for one dimensional chain

have paved a path for the question as to what happens to this "coherent wavefront/pulse" when it propagates through a not so consolidated granular media. With less pre-compression or high wave amplitude; inter-particle forces vary non-linearly with overlap. The inter-particle forces exhibit a departure from the linear towards non-linear nature, in this scenario does the pulse broadening display similar behavior with length or disorder? In the present case, the impulse amplitude has been varied and its effect has been investigated in the following sections. Also, the coherent wavefront has been instrumental in determining the velocity of sound in a medium which is interconnected with bulk and shear moduli, some light has also been shed on this aspect with Hertzian inter-particle forces taken into consideration.

One dimensional chains of particles (Fig. 2) having linear and nonlinear repulsive (Hertzian) interaction forces have been used as models for studying impulse propagation along the chains. The choice of one dimensional chain was motivated by the existence of force chains in granular materials, these force chains act as pathways for sound wave propagation and also support large stresses of the system [12]-[14]. Section II contains the micro-mechanical model of the one-dimensional chain describing the linear and non-linear repulsive interaction forces used in the model, similar model has been used in [10], [15], [16]. The disorder in the system is in the form of mass distribution, it has also been discussed in the afore-mentioned section. Section III contains the numerical results obtained from the simulations of impulse propagation in granular chains, both single realization and ensemble-averaged space time responses have been taken into consideration and discussed upon. Section IV contains the experimental construction of a granular chain using photoelastic elastic discs, it serves as an outlook for experimental validation of numerical results. Section V presents the conclusion along with issues associated with present subject matter requiring further research work.

II. MICROMECHANICAL MODEL: GRANULAR CHAIN

$N + 2$ particles long, pre-compressed granular chain of particles has been taken into consideration. $F_{(i,j)}$ is the repulsive interaction force experienced by neighboring particles i and j, $F_{(i,j)} \propto \delta_{(i,j)}^{(1+\beta)}$, where δ is the non-dimensionalized dynamic inter-particle overlap between the neighboring particles. $\delta_{(i,j)} = \Delta_{(i,j)} - (u^{(j)} - u^{(i)})^{(1+\beta)}$, $\Delta_{(i,j)}$ is the non-dimensionalized initial static overlap due to pre-compression.

$u^{(i)}$ is the non-dimensionalized displacement of the ith particle relative to the initial static pre-compressed state. Hence,

$$F_{(i,j)} = \kappa_{(i,j)}(\Delta_{(i,j)} - (u^{(j)} - u^{(i)}))^{(1+\beta)}, \tag{1}$$

$\kappa_{(i,j)}$ is the non-dimensionalized stiffness.

A. Non-Dimensionalization

The mass of the ith particle $\tilde{m}^{(i)}$ is non-dimensionalized by the mean mass $\tilde{m}_o$, $b^{(i)} \equiv \tilde{m}^{(i)}/\tilde{m}_o$. The stiffness $\kappa_{(i,j)}$ is non-dimensionalized by characteristic stiffness (κ_o; stiffness between same size neighboring particles). The displacement of the ith particle is non-dimensionalized by $\tilde{\Delta}_o$, $u^{(i)} \equiv \tilde{u}^{(i)}/\tilde{\Delta}_o$, where $\tilde{\Delta}_o$ is the initial static overlap when all the particles have uniform characteristic stiffness $\tilde{\kappa}_o$. The initial static overlap for polydisperse particles ($\Delta_{(i,j)}$) is also non-dimensionalized by $\tilde{\Delta}_o$, $\Delta_{(i,j)} \equiv \tilde{\Delta}_{(i,j)}/\tilde{\Delta}_o$. Time is non-dimensionalized by the characteristic time $\tilde{t}_c$, $t \equiv \tilde{t}/\tilde{t}_c$, where $\tilde{t}_c = \sqrt{\frac{\tilde{m}_o}{\tilde{\kappa}_{(i,j)}}}$.

B. Nonlinear Equation of Motion

The nonlinear equation of motion of particle $i = 1$ to N are written as:

$$b^{(i)}\frac{\mathrm{d}^2 u^{(i)}}{\mathrm{d}t^2} = -\kappa_{(i,i+1)}\Big\{\Delta_{(i,i+1)} - (u^{(i+1)} - u^{(i)})\Big\}^{(1+\beta)}$$
$$+\kappa_{(i,i-1)}\Big\{\Delta_{(i,i-1)} - (u^{(i)} - u^{(i-1)})\Big\}^{(1+\beta)} \tag{2}$$

with $u^{(0)}$ and $u^{(N+1)}$ being 0 as the 0th and $N+1^{th}$ particles are fixed.

C. Hertzian Equation of Motion

Substituting $\beta = 1/2$ in (2) gives the Hertzian equation of motion [17]

$$b^{(i)}\frac{\mathrm{d}^2 u^{(i)}}{\mathrm{d}t^2} = -\kappa_{(i,i+1)}\Big\{\Delta_{(i,i+1)} - (u^{(i+1)} - u^{(i)})\Big\}^{(3/2)}$$
$$+\kappa_{(i,i-1)}\Big\{\Delta_{(i,i-1)} - (u^{(i)} - u^{(i-1)})\Big\}^{(3/2)} \tag{3}$$

which is valid for repulsive interactions between spherical particles. Equation (3) is solved numerically using Verlet integration scheme. Verlet has been used because of its symplectic nature.

1) *Hertz Contact Model:* For the nonlinear repulsive interaction between the particles to be Hertzian, the non-dimensionalised contact stiffness is given by [10], [17]

$$\tilde{\kappa}_{(i,j)} = \frac{\tilde{\kappa}_{(i,j)}}{\tilde{\kappa}_o} = \sqrt{\frac{2}{b^{(i)} + b^{(j)}}}\Big(b^{(i)}b^{(j)}\Big)^{(1/6)}. \tag{4}$$

The characteristic time is

$$\tilde{t}_c = \frac{1}{\Delta_o}^{1/4}\sqrt{\frac{1-\nu^2}{\tilde{E}}}\left[\frac{243\pi\tilde{\rho}\tilde{m}_o^5}{2}\right]^{1/12}. \tag{5}$$

The initial overlap during static equilibrium is given by

$$\Delta_{(i,j)} = \frac{\tilde{\Delta}_{(i,j)}}{\tilde{\Delta}_o} = \kappa_{(i,j)}^{-2/3} \tag{6}$$

D. Linearized Equation of Motion

Equation (1) can be expressed as a power series about the initial overlap ($\Delta_{(i,j)}$),

$$F_{(i,j)} = \kappa_{(i,j)}\Delta_{(i,j)}^{1+\beta} + \kappa_{(i,j)}(1+\beta)\Delta_{(i,j)}^{\beta}(\delta_{(i,j)} - \Delta_{(i,j)})$$
$$+ \frac{1}{2}\kappa_{(i,j)}\beta(1+\beta)\Delta_{(i,j)}^{\beta-1}(\delta_{(i,j)} - \Delta_{(i,j)})^2 + \dots \quad (7)$$

For small amplitudes of wave propagation (in present scenario, an initial impulse, v_o), the displacement of particles from the initial static overlap condition is small, this can be used to ignore higher order terms in (7) resulting in

$$F_{(i,j)} = \kappa_{(i,j)}\Delta_{(i,j)}^{1+\beta} - \kappa_{(i,j)}(1+\beta)\Delta_{(i,j)}^{\beta}\left(u^{(j)} - u^{(i)}\right). \quad (8)$$

Now, (8) can be used to arrive at linearized equation of motion for a particle i,

$$b^{(i)}\frac{\mathrm{d}^2 u^{(i)}}{\mathrm{d}t^2}$$
$$= \kappa_{(i-1,i)}\Delta_{(i-1,i)}^{\beta}\left[\Delta_{(i-1,i)} - (1+\beta)(u^{(i)} - u^{(i-1)})\right] \quad (9)$$
$$- \kappa_{(i+1,i)}\Delta_{(i,i+1)}^{\beta}\left[\Delta_{(i+1,i)} - (1+\beta)(u^{(i+1)} - u^{(i)})\right].$$

Using $\beta = 1/2$ and (6) we get linearized hertzian equation of motion

$$\frac{b^{(i)}}{(1+\beta)}\frac{\mathrm{d}^2 u^{(i)}}{\mathrm{d}t^2} = \kappa_{(i+1,i)}^{2/3}(u^{(i+1)} - u^{(i)}) \quad (10)$$
$$- \kappa_{(i-1,i)}^{2/3}(u^{(i)} - u^{(i-1)})$$

Equation (10) for particles $i = 1$ to $i = N$ can be assembled in the form of an equation consisting of matrices resulting in

$$\mathbf{M}\frac{\mathrm{d}^2\mathbf{u}}{\mathrm{d}t^2} = \mathbf{K}\mathbf{u} + \mathbf{f}, \quad (11)$$

where $\mathbf{M}$ is the mass matrix with diagonal entries $b^{(1)}$, $b^{(2)}$, $b^{(3)}$, ..., $b^{(N)}$ and zero otherwise, $\mathbf{K}$ is the stiffness matrix with diagonal entries $-(\kappa_{(i+1,i)} + \kappa_{(i-1,i)})/(1 + \beta)$, superdiagonal $(\kappa_{(i+1,i)}/(1 + \beta))$ and subdiagonal $(\frac{\kappa_{(i-1,i)}}{(1+\beta)})$ elements. $\mathbf{f}$ is the external force. For impulse driving, $\mathbf{f} = 0$, initial displacement vector of particles $\mathbf{u}_o = [0\ 0\ ...\ 0]$ and initial velocity vector of particles $\mathbf{v}_o = [v_o\ 0\ ..\ 0]$ (the first particle receiving the impulse). Substituting $\mathbf{A} = -\mathbf{M}^{-1}\mathbf{K}$ and using ansatz $\mathbf{u} = \mathbf{u}'e^{i\omega t}$ (assuming plane wave motion of particles) gives

$$\mathbf{A}\mathbf{u} = \omega^2\mathbf{u}. \quad (12)$$

The solution of this equation can be expressed as a superposition of eigenmodes,

$$\mathbf{u} = \mathbf{S}\mathbf{C}^{(1)}\mathbf{G}^{-1}\mathbf{S}^{-1}\mathbf{v}_o + \mathbf{S}\mathbf{C}^{(2)}\mathbf{S}^{-1}\mathbf{u}_o, \quad (13)$$

where $\mathbf{S}$ is the eigenbasis matrix of $\mathbf{A}$ and contains eigenvectors $\mathbf{s}_j$ as column vectors. Each eigenvector has a respective eigenvalue ω_j^2 associated with it (ω_j is the eigenfrequency). The set of eigenvectors are orthonormalized by the orhtonormality condition $\mathbf{s}_{(i)}^{\mathrm{T}}\mathbf{M}\mathbf{s}_{(j)} = \delta_{(i,j)}$ where $\delta_{(i,j)}$ is the Kronecker delta function. Hence, the displacements individual particles are given by

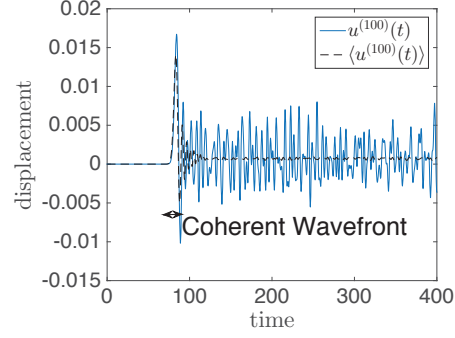$$u^{(i)}(t) = v_o\sum_{j=1}^{N}\frac{S_{ij}S_{1j}\sin(\omega_{(j)}t)}{\omega_{(j)}}. \quad (14)$$

Fig. 3 Wave propagating in a one-dimensional chain, single and ensemble averaged displacement response of 100th particle, initial impulse $v_o = 0.1$, disorder $\xi = 0.2$

E. Disorder in the Chains and Ensemble Averaging

The masses of the particles in the granular chains $b^{(i)}$ have been selected randomly from a normal distribution.

$$f^{(n)}(b) = \frac{1}{\xi\sqrt{2\pi}}e^{\frac{(b-1)^2}{2\xi^2}}, \quad (15)$$

where $f^{(n)}(b)$ is the probability distribution function of the mass distribution. The mean of the distribution is 1 and its standard deviation is ξ, the disorder parameter of the chain. A similar disorder model has been used in [10], [15], [18]; this disorder model has also been termed "diagonal randomness" [4] because the diagonal elements of the mass matrix $\mathbf{M}$ are the masses of the particles (Section II-D). In [10] and [15], it has been observed that the space time responses of the particles in different disordered chains are quantitatively similar if the first two moments of the mass distributions are the same. To obtain a coherent picture of space time responses (coherent wavefront without the multiply scattered part of the wave), ensemble averaging has been used. Multiple realizations of chains have been averaged with the same disorder parameter and the same impulse amplitude to study the coherent wavefront propagation characteristics. $\langle\rangle$ is used to represent ensemble averaged physical quantities, e.g. $\langle u^{(i)}(\tau)\rangle$ represents the ensemble averaged space time displacement response.

III. NUMERICAL RESULTS AND DISCUSSIONS

Equations (3) and (14) have been used to numerically and analytically compute space time responses for 512 particles long granular chains for different disorder parameters (ξ) and for different impulse amplitudes (v_o). The space time responses for single realizations as well as for ensembles with the same ξ are used for analysis. The output time step $\Delta t = 9.7656 \times 10^{-4}$ and the maximum time period is 512 units.

A. Ensemble Averaged Space Time Responses and the Coherent Wavefront

Fig. 3 shows the displacement response of the 100th particle in a 512 particles long granular chain for a single realization as well as for ensemble averaged 500 realizations. Ensemble
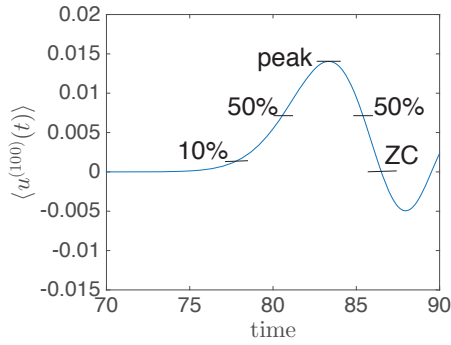
Fig. 4 Coherent wavefront of the displacement response of 100th particle (zoomed version; see Fig. 1), initial impulse $v_o = 0.1$, $\xi = 0.2$
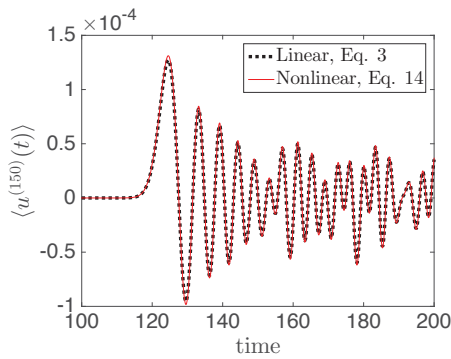

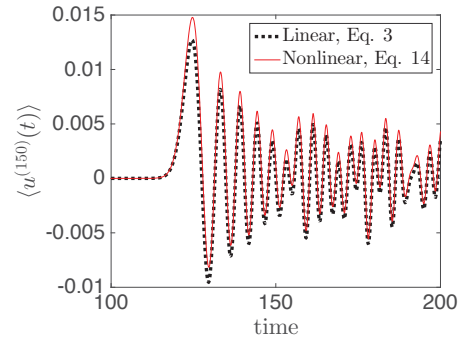Fig. 6 Displacement response of 150th particle given by (3) and (14), $v_o = 0.1$, $\xi = 0.1$

Fig. 5 Displacement response of 150th particle given by (3) and (14), $v_o = 0.001$, $\xi = 0.1$
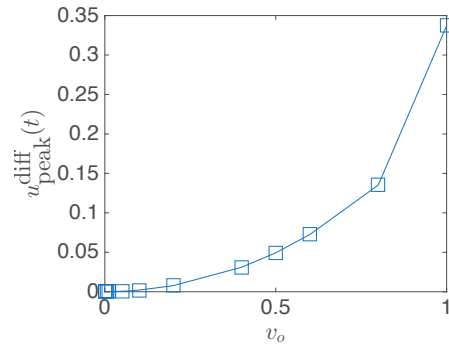

Fig. 7 Difference between the **peak** amplitudes of the coherent wavefront calculated by (3) numerically and (14) analtically for 150th particle, $\xi = 0.1$

averaging removes the coda, but the coherent wavefront is preserved. As mentioned in Section I, ensemble averaging improves the quality of the coherent wavefront signal which then can be utilized for determining bulk parameters of the material. For further studying the coherent wavefront, it has been characterized by various points as illustrated in Fig. 4; a similar methodology has been used previously [5], [10], [19].

The point **peak** signifies the point at which the coherent wavefront achieves the maximum value, **50%** signifies the point at which it achieves 50% of the maximum value, and similarly with **10%**. **ZC** signifies the point at which the wavefront crosses zero for the first time after achieving its maximum value (peak). As it can be observed from Fig. 4, the points **10%** and **50%** lie on both the sides of the peak of the coherent wavefront; this property is instrumental in measuring the width of the coherent wavefront, the width associated with 50% is also denoted as the Full Width Half Maxima (FWHM) and half of the width at 50% is referred to as Half Width at Half Maxima (HWHM) [20].

B. Linear vs. Nonlinear Space Time Responses

Figs. 5 and 6 show the displacement response of the 150th particle belonging to granular chains with the same disorder parameter ($\xi = 0.1$), however with different impulse amplitudes, $v_o = 0.001$ and $v_o = 0.1$ respectively. It can be observed that the difference between space time responses

from (3) and (14) is more significant in Fig. 6 indicating enhanced nonlinearity with increase in impulse amplitude. Fig. 7 shows the difference between the peak amplitudes ($u_{\text{peak}}^{\text{diff}}$) of the coherent wavefront of the space time responses of the 150th particle, obtained from Eq. (3) (nonlinear, numerical) and Eq. (14) (linearized, analytical). Similar observations were also made in [10]. The width of the coherent wavefront for different impulse amplitudes (v_o) will be evaluated next.

C. Width of the Coherent Wavefront

The width of the coherent wavefront will be evaluated in this section for an ordered chain, a disordered chain and then for different impulse amplitudes after adopting a framework for re-scaling the time and amplitude.

1) Re-Scaling Time and Amplitude: The framework is similar to the one adopted in [5], it aids in comparing across different simulation parameters as well as with experimental results. Time and amplitude are scaled by the time of arrival (t_{peak}) and the amplitude (A_{peak}) of the coherent wavefront, respectively. The width of the coherent wavefront for HWHM (50%) is defined as

$$W = \frac{t_{\text{peak}} - t_{50\%}}{t_{\text{peak}}}, \qquad (16)$$

where t_{peak} is the time of arrival or the time at which the coherent wavefront achieves its maximum value, while $t_{50\%}$ is the time at which the coherent wavefront's amplitude is 50% of the maximum amplitude.
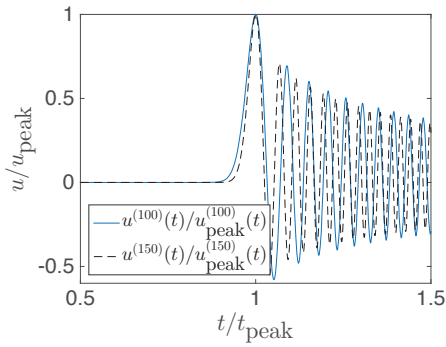
Fig. 8 Amplitude and time scaled displacement response of 100th and 150th particles, $v_o = 0.1$, with order $\xi = 0.0$
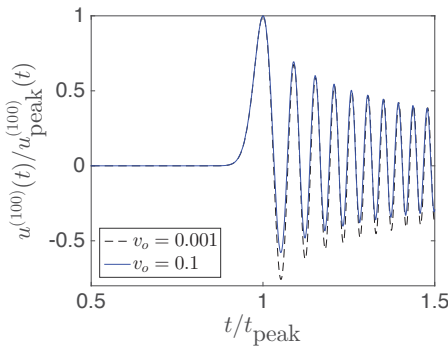

Fig. 9 Amplitude and time scaled displacement response of 100th particle when $v_o = 0.001$ and $v_o = 0.1$, $\xi = 0.0$
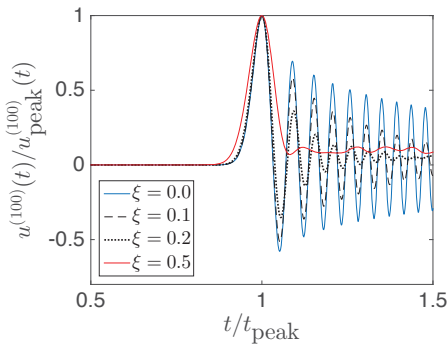

Fig. 10 Amplitude and time scaled displacement response of 100th particle for different disorder parameters

Fig. 11 Scaled width (W) of the coherent wavefront for an ordered and disordered chains with distance i from the source. $v_o = 0.1$

Fig. 12 Scaled width (W) of the coherent wavefront for an ordered and a disordered chain ($\xi = 0.2$) with distance i from the source., for varying impulse amplitudes v_o

2) Ordered Chain: Fig. 8 contains the amplitude and time scaled displacement response of two different particles along a granular chain, it can be observed that the time of arrival of the coherent wavefront as well as the amplitude have collapsed but not the width. Fig. 9 shows the re-scaled displacement responses of 100th particle for different v_o, showing a perfect collapse of the coherent wavefront with same peak amplitude, time of arrival and width as well, indicating that the impulse amplitude has no effect on width (W) of the coherent wavefront in an ordered chain.

3) Disordered Chain: Fig. 10 displays the space time responses of the 100th particle for different disorder parameters ($\xi = 0.0$, $\xi = 0.1$, $\xi = 0.2$ and $\xi = 0.5$, with $v_o = 0.1$).
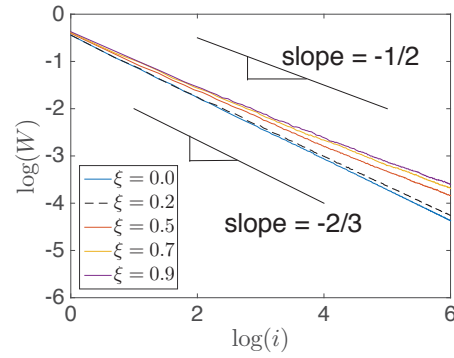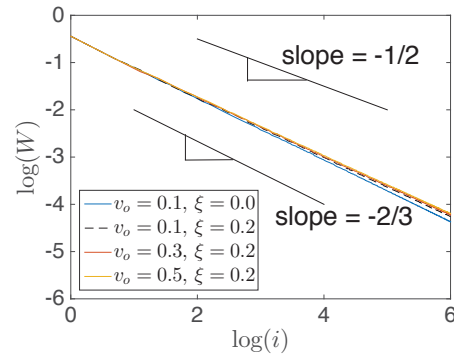
The coherent wavefront collapses completely after scaling for small disorder parameters but, as the disorder increases, the width increases too, indicating that the disorder parameter has a role to play in the width of the coherent wavefront.

4) Width of the Coherent Wavefront: In Ref. [5], it was observed that for ordered chains the scaled width (W) of the coherent wavefront decreases from the distance from the source following a power law relationship, $W \propto L^{-2/3}$ which can be observed in our model as well (Fig. 11). In [5] it was proposed that all disordered chains have a coherent wavefront propagating with power law relationship of $W \propto L^{-1/2}$. We can see from Fig. 11 that for slightly disordered media (e.g. $\xi = 0.1, 0.2$), the power law exponent is $-2/3$, but the exponent lies between $-2/3$ and $-1/2$ for stronger disorder and further increase in disorder makes the exponent approach $-1/2$. From Fig. 12 it can be observed that v_o has not much effect on W. The coherent wavefront is a little sensitive to large or small impulse amplitudes.

D. Coherent Wavefront Velocity

The velocity of the coherent wavefront's peak can be calculated by dividing the individual particle number (i) with the time of arrival t_{peak}. Fig. 13 shows these results for granular chains with different disorder parameters and Fig. 14 for granular chains experiencing different impulse amplitudes. In both figures, an acceleration close to the source can be observed
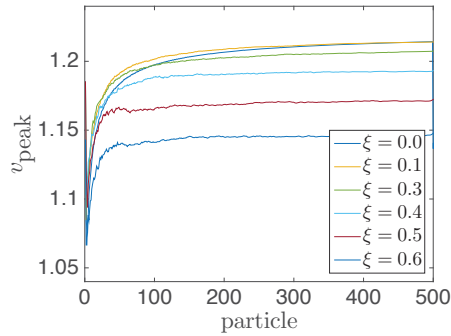
Fig. 13 Velocity of the peak of coherent wavefront for different particles in a granular chain with varying disorder parameter ξ
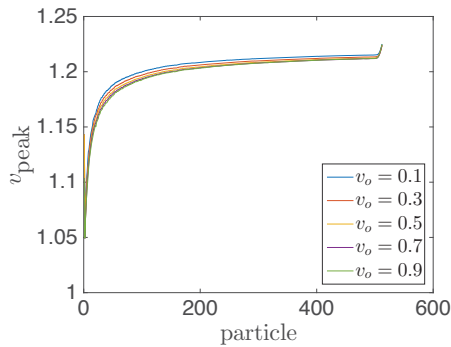

Fig. 14 Velocity of the peak of coherent wavefront for different particles in a granular chain with varying impulse amplitude v_o
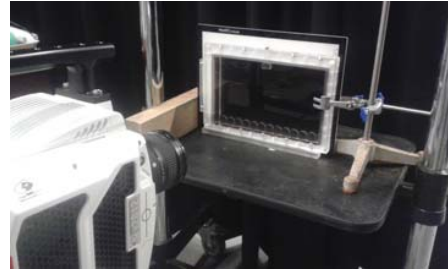

Fig. 15 Experimental setup
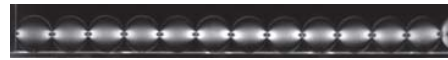

Fig. 16 Lit experimental setup

Fig. 17 One dimensional chain of photoelastic particles

Fig. 18 One dimensional chain of photoelastic particles with marked circular boundaries of particles

which was also reported in Refs. [10] and [21]. It is also observed that an increase in either disorder or impulse velocity decreases v_{peak}. However, the effect of impulse velocity (v_o) is not very significant.

E. Experimental Construction: An Outlook

To validate the theory described above, the simulations can be reproduced experimentally using discs made out of a photoelastic material, Clear Flex 50 (*Smooth-on*), to measure the forces at the contacts. Figs. 15 and 16 show different views of the experimental setup. A chain of 12 photoelastic discs, 2cm in diameter and 0.6cm deep, were lined up on the bottom of an acrylic container 26cm wide, 17cm high and 0.8cm in depth, one of whose sides was free to move horizontally and act as a plunger on the chain of discs. This container was lit from behind by a *MiniSun* A4 LED LightPad, and between them a red filter was placed to narrow the range of wavelengths of the light that passed through the photoelastic material. Two opposite circular polarizers were attached on either side of the container, one between the red filter and the first acrylic wall and the second between the other side and a high-speed camera. Thus, the second polarizer would cancel all the light that passes through the first one except for that which was affected by the photoelastic response of the compressed discs. Fig. 16 shows the setup when the LightPad is turned on. The acrylic container seems dark due to the opposite polarizers, except for regions within the discs where some red light is transmitted because of the materials photoelastic response to compression. Fig. 17 is an example image taken by the camera in this setup. Before an experiment, a heavy block of wood was leaned against the plunger to provide an arbitrary load on the chain of discs. Through a soft tap on the plunger, a pulse can be introduced into the pre-compressed chain, and its progress along the chain can be recorded by the camera. Preliminary experiments show that the pulse takes only a few milliseconds to be transmitted along a disc, so experiments can be recorded at a frame rate of 10000 frames per second to ensure sufficient spatial and temporal resolution. The forces at the contacts on either side of each particle are then computed in the post-processing of each frame.

F. Force Measurements and Moving Average Filter

First, the measurement of the forces at the contacts between discs was attempted here as a function of their overlap when under compression. At the disc edges there is a noticeable intensity gradient, and a Hough Transform is applied to each frame returning the centre positions and radii of the circles with brightest circumference. Fig. 18 superimposes in red the result of this algorithm - the locations and sizes of twelve circles - onto a sample experimental image. The discs are numbered from one to twelve from left to right (in the order in which the pulse travels across them). It can be seen here that the red circles would appear to coincide well
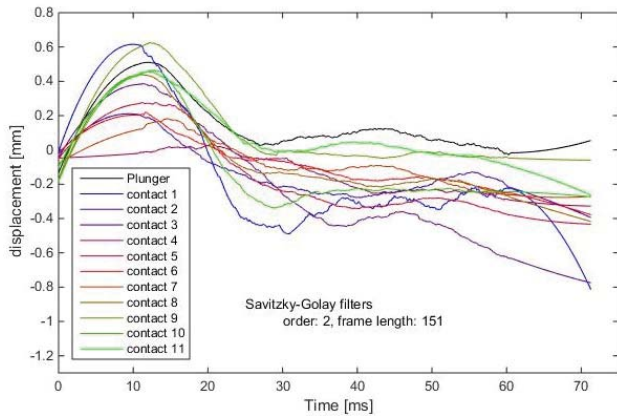
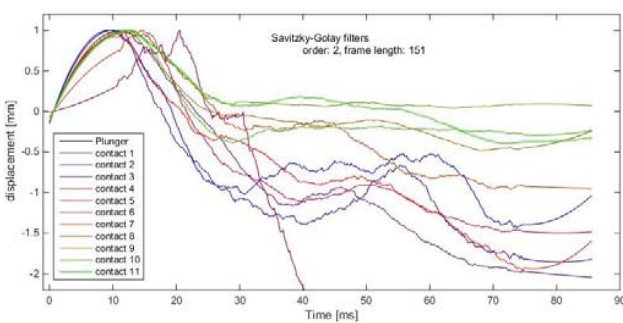Fig. 19 Moving average filtered displacement response

Fig. 20 Nomalized, moving average filtered displacement response

with the visible disc edges, because the compression at the contacts is small and does not affect the circularity of most of the discs. Although the discs are under compression, the overlaps between them are only barely perceptible by eye, but the circle-finding method is precise enough to detect a sub-pixels at each contact. The recorded overlaps are unfortunately extremely noisy because the disc edges can be multiple pixels thick at some places (due to refraction of the background light and to slight parallax error in some cases) and the Hough Transform's decision on where the circumference lies changes slightly from frame to frame, it significantly affects the small measured overlap between circles. Nevertheless, by applying a moving average filter to the raw data (Fig. 19) a definite increase in the compression can be measured as the plunger (black line) pushes inwards and compresses the chain. The absolute values of the overlap are a little different at each contact because of a parallax error, but if these are normalized (Fig. 20), the compression peaks show a subtle shift from contact to contact in the same order as they are numbered at least qualitatively confirming the simulations.

IV. CONCLUSION

The coherent wavefront is the long wavelength and low frequency part of a sound signal propagating in granular media. Its short wavelength and high frequency counterpart "coda" is composed of multiply scattered waves, forming the significant part of the sound signal. Thus, on ensemble averaging, the coda gets completely washed out. An elementary granular chain of spherical particles with both linear and nonlinear repulsive interaction forces has been used as a model (Section II) to study the shape and propagation characteristics of the coherent wavefront. The masses of the particles were selected randomly from a normal distribution, the standard deviation of this distribution quantifies the disorder parameter (Section II-E). Both single realizations and displacement responses averaged over various samples were chosen for analysis. The space time responses calculated by the nonlinear equation of motion (3) and by the analytical solution of the linearized equation of motion (14) exhibited a significant difference only for larger impulse amplitudes (Figs. 5 and 6), increasing exponentially with impulse magnitude (Fig. 7). The time and amplitude were re-scaled according to the methodology used in [5] for further analysis (Fig. 8 and 9). Half Width at Half Maximum (HWHM) of the coherent wavefront was used to quantify its scaled width. W decreases with distance from the source following a power law relationship $W \propto L^{-2/3}$ for an ordered chain (Fig. 11). However, for disordered chains the power law exponent starts increasing with increasing disorder parameter and tends to approach -1/2 (Fig. 12). Change in impulse magnitude (v_o) has no strong effect on the aforementioned power law relationship. The peak velocity of the coherent wavefront (v_{peak}) was also measured and it was observed that increase in disorder considerably decreases the peak velocity and increase in impulse magnitude slightly decreases the peak velocity (Figs. 13 and 14). An experimental set-up of a granular chain comprising of photoelastic disks was also discussed to validate or challenge the numerical results. The framework of moving average filters to improve signal to noise ratio was also laid down but warrants further study.

The power law relationship exhibited by the coherent wavefront can be exploited to know the structure or disorder of the system through which sound signals propagate. The attenuation of the coherent wavefront got removed due to the scaling of the amplitude, but its connection with multiple scattering and hence, the coda require further study.

REFERENCES

[1] P. Shearer, *Introduction to Seismology*. Cambridge University Press, 2009. (Online). Available: https://books.google.nl/books?id=VV0mV4lF0RUC.
[2] A. M. Dainty and M. Toksz, "Seismic codas on the earth and the moon: a comparison," *Physics of the Earth and Planetary Interiors*, vol. 26, no. 4, pp. 250 – 260, 1981. (Online). Available: http://www.sciencedirect.com/science/article/pii/0031920181900297.

[3] J. O'Donovan, E. Ibraim, C. O'Sullivan, S. Hamlin, D. Muir Wood, and G. Marketos, "Micromechanics of seismic wave propagation in granular materials," *Granular Matter*, vol. 18, no. 3, p. 56, Jun 2016. (Online). Available: https://doi.org/10.1007/s10035-015-0599-4.

[4] P. Sheng, *Intoduction to Wave Scattering, Localization and Mesoscopic Phenomena*, ser. Springer Series in Materials Science. Springer, 2006. (Online). Available: https://doi.org/10.1007/3-540-29156-3.

[5] V. Langlois and X. Jia, "Sound pulse broadening in stressed granular media," *Phys. Rev. E*, vol. 91, p. 022205, Feb 2015. (Online). Available: https://link.aps.org/doi/10.1103/PhysRevE.91.022205

[6] I. Güven, "Hydraulical and acoustical properties of porous sintered glass bead systems: experiments, theory, & simulations," Ph.D. dissertation, Enschede, 2016. (Online). Available: http://doc.utwente.nl/100546/.

[7] X. Jia, "Codalike multiple scattering of elastic waves in dense granular media," *Phys. Rev. Lett.*, vol. 93, p. 154303, Oct 2004. (Online). Available: http://link.aps.org/doi/10.1103/PhysRevLett.93.154303.

[8] X. Jia, C. Caroli, and B. Velicky, "Ultrasound propagation in externally stressed granular media," *Phys. Rev. Lett.*, vol. 82, pp. 1863–1866, Mar 1999. (Online). Available: http://link.aps.org/doi/10.1103/PhysRevLett.82.1863.

[9] H. A. Makse, N. Gland, D. L. Johnson, and L. Schwartz, "Granular packings: Nonlinear elasticity, sound propagation, and collective relaxation dynamics," *Phys. Rev. E*, vol. 70, p. 061302, Dec 2004. (Online). Available: http://link.aps.org/doi/10.1103/PhysRevE.70.061302.

[10] R. K. Shrivastava and S. Luding, "Effect of disorder on bulk sound wave speed: a multiscale spectral analysis," *Nonlinear Processes in Geophysics*, vol. 24, no. 3, pp. 435–454, 2017. (Online). Available: https://www.nonlin-processes-geophys.net/24/435/2017/.

[11] V. Nesterenko, "Propagation of nonlinear compression pulses in granular media," *J. Appl. Mech. Tech. Phys.*, vol. 24, pp. 733–743, March 1983.

[12] E. T. Owens and K. E. Daniels, "Sound propagation and force chains in granular materials," *EPL (Europhysics Letters)*, vol. 94, no. 5, p. 54005, 2011. (Online). Available: http://stacks.iop.org/0295-5075/94/i=5/a=54005.

[13] E. Somfai, J.-N. Roux, J. H. Snoeijer, M. van Hecke, and W. van Saarloos, "Elastic wave propagation in confined granular systems," *Phys. Rev. E*, vol. 72, p. 021301, Aug 2005. (Online). Available: http://link.aps.org/doi/10.1103/PhysRevE.72.021301.

[14] T. S. Majmudar and R. P. Behringer, "Contact force measurements and stress-induced anisotropy in granular materials," *Nature*, vol. 435, no. 1079, pp. 1079–1082, 06 2005. (Online). Available: http://dx.doi.org/10.1038/nature03805.

[15] B. P. Lawney and S. Luding, "Massdisorder effects on the frequency filtering in onedimensional discrete particle systems," *AIP Conference Proceedings*, vol. 1542, no. 1, pp. 535–538, 2013. (Online). Available: http://scitation.aip.org/content/aip/proceeding/aipcp/10.1063/1.4811986.

[16] Shrivastava, Rohit Kumar and Luding, Stefan, "Wave propagation of spectral energy content in a granular chain," *EPJ Web Conf.*, vol. 140, p. 02023, 2017. (Online). Available: https://doi.org/10.1051/epjconf/201714002023.

[17] L. D. Landau and E. M. Lifshitz, *Theory of elasticity*. Pergamon Press, 1970.

[18] P. W. Anderson, "Absence of diffusion in certain random lattices," *Phys. Rev.*, vol. 109, pp. 1492–1505, Mar 1958. (Online). Available: http://link.aps.org/doi/10.1103/PhysRev.109.1492.

[19] J. O'Donovan, C. O'Sullivan, G. Marketos, and D. Muir Wood, "Analysis of bender element test interpretation using the discrete element method," *Granular Matter*, vol. 17, no. 2, pp. 197–216, 2015. (Online). Available: http://dx.doi.org/10.1007/s10035-015-0552-6.

[20] E. W. Weisstein, "Tree. From MathWorld—A Wolfram Web Resource," last visited on 6/9/2017. (Online). Available: http://mathworld.wolfram.com/GaussianFunction.html.

[21] O. Mouraille, W. A. Mulder, and S. Luding, "Sound wave acceleration in granular materials," *Journal of Statistical Mechanics: Theory and Experiment*, vol. 2006, no. 07, p. P07023, 2006. (Online). Available: http://stacks.iop.org/1742-5468/2006/i=07/a=P07023.